Tellus
SERIES B
CHEMICAL
AND PHYSICAL
METEOROLOGY
PUBLISHED BY THE INTERNATIONAL METEOROLOGICAL INSTITUTE IN STOCKHOLM

Tellus (2011), 63B, 512–530
Printed in Singapore. All rights reserved

TELLUS

Individual-particle analysis of airborne dust samples collected over Morocco in 2006 during SAMUM 1

By D. SCHEUVENS[1,2]*, K. KANDLER[2], M. KÜPPER[2], K. LIEKE[2], S.R. ZORN[3], M. EBERT[2], L. SCHÜTZ[1] and S. WEINBRUCH[2], [1]*Institut für Physik der Atmosphäre, Johannes-Gutenberg-Universität, J.-J.-Becherweg 21, 55099 Mainz, Germany;* [2]*Institut für Angewandte Geowissenschaften, Technische Universität Darmstadt, Schnittspahnstraße 9, 64287 Darmstadt, Germany;* [3]*School of Engineering and Applied Sciences, Harvard University, 58 Oxford Street, Cambridge, MA 02138, USA*

(Manuscript received 19 November 2010; in final form 11 May 2011)

ABSTRACT

During the course of SAMUM 1 in May and June 2006, airborne samples were collected in southern Morocco at altitudes between 830 and 3340 m above ground. We analysed approximately 22 500 particles of 1–30 μm by automated individual-particle analysis with a scanning electron microscope (SEM) and an energy-dispersive X-ray (EDX) analyser. The major difference between samples is due to the presence and amount of chlorine- and sulphur-bearing particles, pointing to a varying maritime influence and to different degrees of aging. In contrast, the desert dust component is very homogeneous independent of altitude, activated local source area, and dust storm intensity, implying very fast mixing of the entrained dust with a persistent regional background aerosol. Nevertheless, our study reinforces the usefulness of carbonates and palygorskite as 'compositional fingerprints' for mineral dust from source areas in northwestern Africa.

The average median aspect ratio of most particle groups is in the range between 1.5 and 1.6. Higher values are found for S- and Cl-dominated particles (except sodium chloride), and internal mixtures of alumosilicates with carbonates or sulphates. Taken together with other studies, a tendency of increasing aspect ratios with longer transport distances can be observed for Saharan dust.

1. Introduction

Northern African mineral dust represents about one half of the Earth's total mineral dust burden (Engelstaedter et al., 2006; Laurent et al., 2008). The input of Saharan/Sahelian dust and associated nutrients as iron and phosphorus into Earth's atmosphere and subsequent deposition after long-range transport has severe consequences on terrestrial and marine ecosystems (Arimoto, 2001) in far-off regions such as the Amazon basin (Swap et al., 1992), the Atlantic ocean including the Caribbean region (Jickells et al., 2005) or the Mediterranean (Guieu et al., 2002). The entrainment of northern African dust also causes more local effects in the vicinity of the source regions (e.g. negative health effects on the local population, soil degradation, visibility reduction and/or damage on transport systems and machinery; e.g. Ozer et al., 2006; see also Goudie and Middleton, 2006). Another important issue is the influence of mineral dust on the Earth's climate system. Input of dust particles into the atmosphere changes the radiative budget by direct effects through scattering and absorption of both, the solar and terrestrial radiation, and by indirect effects in providing cloud condensation and ice nuclei (Sokolik et al., 2001; IPCC, 2007). Mineral dust acts as a sink for trace gases of the atmosphere through heterogeneous reactions (Dentener et al., 1996) and probably interferes with the formation of tropical cyclones over the Atlantic Ocean (Wu, 2007). Furthermore, Saharan dust transported to the north is responsible for the exceedance of PM_{10} levels of the daily limits in the Mediterranean region (e.g. Nicolás et al., 2008).

The impacts of mineral dust on the climatic system depend largely on the physical (grain size distribution, particle shape and morphology) and chemical (mineralogy, mixing state) properties of the dust, and hence a detailed characterization of different mineral dust types is necessary for its implementation in recent and future climate models. Many climate models assume that mineral dust in the atmospheric column is homogeneous from Earth's surface to its top, despite the fact that for example different studies in the western part of northern Africa showed an

*Corresponding author.
e-mail: dscheuvens@geo.tu-darmstadt.de
DOI: 10.1111/j.1600-0889.2011.00554.x

impressive stratification and layering of the dust content in the atmosphere (e.g. Formenti et al., 2003; Berthier et al., 2006; Lieke et al., 2011).

In the last 30 yr, different studies using a large range of source identification methods (e.g. visibility studies, different remote sensing methods) showed that in northern Africa the entrainment of dust is largely restricted to specific regions, so-called potential source areas (e.g. d'Almeid, 1986; Prospero et al., 2002; Laurent et al., 2008; Schepanski et al., 2009). Important potential source areas in northern Africa are for example the Bodélé depression in the Chad basin, a region to the west of the Hoggar mountains at the Algerian–Mali border, the coast of Western Sahara, the foothills of the Atlas mountains, the zone of chotts in northern Algeria and Tunisia, and areas in central Libya and at the border region of Egypt and Somalia. Bulk mineralogical, isotope and chemical data of dust and sediment samples from the different source regions reveal that source sediments significantly vary in their composition, but if these differences in composition are still detectable after long- to medium-range transport and subsequent sedimentation is still a matter of debate (Brust and Waniek, 2010).

Besides the above-mentioned bulk analytical methods, in recent years the characterization of mineral dusts by individual-particle analysis became an important tool with the advantage to obtain additional information on parameters such as grain size distribution, particle shape and internal mixing state (e.g. Moreno et al., 2006; Chou et al., 2008; Kandler et al., 2007, 2009, 2011; Matsuki et al., 2010; Kandler et al., 2011; Lieke et al., 2011).

The first part of the Saharan Mineral Dust Experiment (SAMUM 1) was conducted in Morocco in May and June 2006 and was dedicated to understand the physical and chemical characteristics and radiative effects of mineral dust close to a source region (Heintzenberg, 2009). The availability of two aircrafts offered the possibility to obtain airborne samples for individual-particle analysis on different sampling days. During the course of SAMUM 1, three major dust and two transitional phases occurred (Knippertz et al., 2009): dust episode 1 from 12 to 15 May, intermediate phase 1 from 16 to 21 May, dust episode 2 from 22 to 27 May, intermediate phase 2 from 28 to 30 May, and dust episode 3 from 31 May to 7 June. Whereas the first and the second dust phase are characterized by a well-mixed dust layer structure at Ouarzazate (southern Morocco), the third dust event is coupled with a two-layer structure with a boundary located at about 2800 m a.s.l. A combination of back-trajectory analysis and analysis of meteorological and remote sensing data shows that during the three dust episodes different source areas were activated (Petzold et al., 2009). Mineral dust was uplifted either in central and western Algeria (dust episode 1 and dust episode 2) or in northern Algeria along the foothills of the Atlas Mountains and in the zone of chotts at the border of Algeria and Tunisia (episode 3). Furthermore, an additional local component by uplift of dust in the vicinity of Ouarzazate has to be taken into account (Fig. 1).

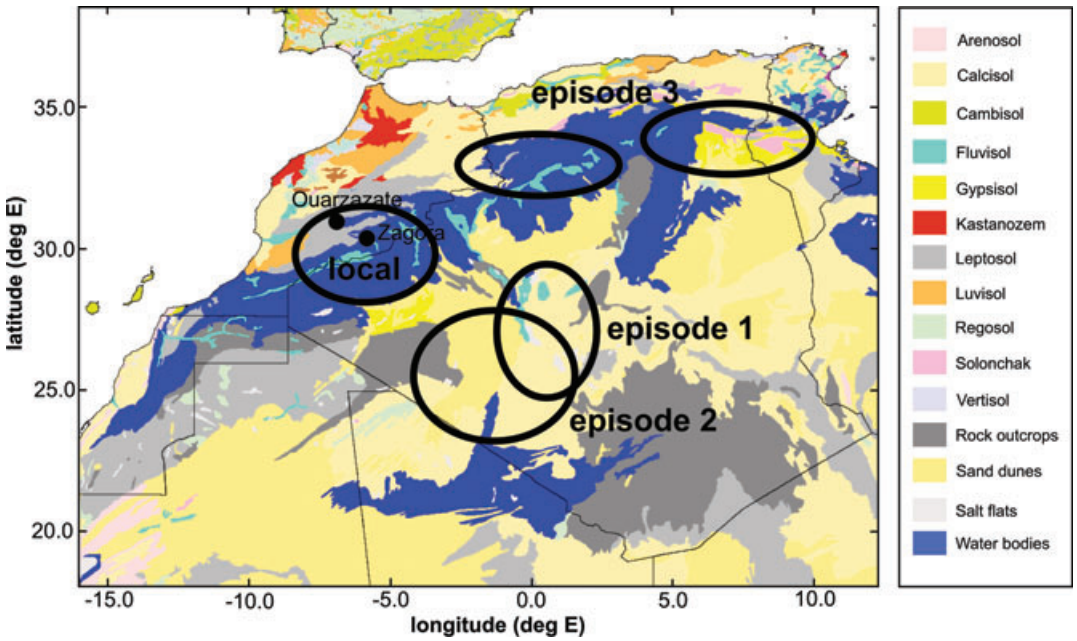

Fig. 1. Study area with location of Ouarzazate (base for the Partenavia flights) and Zagora in southern Morocco; black ellipses mark possible source regions for the three different dust episodes encountered during the course of SAMUM 1 (adapted from Petzold et al., 2009); background soil map was produced with Harmonized World Soil Database Viewer (HWSD viewer) (FAO/IIASA/ISRIC/ISSCAS/JRC, 2009), topsoils with a $CaCO_3$ content >25% are highlighted in blue.

This paper presents compositional data obtained by automated individual-particle analysis from one intermediate and two dust episodes and above and below the boundary of the two-layer structure of episode 3. The collection of samples in different altitudes within a short time period of several hours enables the characterization of the composition of mineral dust in an atmospheric column between about 800 and 3500 m altitude above ground. In combination with back-trajectory analysis this paper intends to answer the following questions:

What is the composition of airborne-sampled mineral dust close to the source regions in the northernmost part of Africa and what are the average shape parameters (aspect ratio, shape factor) of the different components (particle groups)? How does the dust composition differ from sampling day to sampling day and/or between different dust episodes? How does the composition of mineral dust change with altitude during a single dust event? What is the internal mixing state of mineral dust after short- to medium-range transport?

2. Methods

During the SAMUM 1 field experiment (see Knippertz et al., 2007; Heintzenberg, 2009 for a detailed description of the study area), airborne particulate samples were collected with an automatic Mobile Cascade Impaction System (MOCIS) under isokinetic aspiration conditions operated in an underwing pod attached to the 'Partenavia P68B' research aircraft. The MOCIS (Matthias-Maser, 1999; Weigel, 2002; Zorn, 2005) is a cascade impaction system providing aerosol samples within five size ranges above 0.4 μm aerodynamic diameter. Sampling was carried out in the region over Ouarzazate and Zagora between 19 May and 5 June 2006, generally between 8 and 12 a.m., and covered intermediate episode 1 (19 and 20 May 2006), dust episode 2 (27 May 2006) and dust episode 3 (3 and 5 June 2006). Sampling altitudes were between about 800 and 3350 m above ground. These heights are always below the top of the dust layer on the different sampling days, which typically reaches 4–6 km altitude a.s.l. (Tesche et al., 2009; Weinzierl et al., 2009). Particles were collected on a pure carbon adhesive substrate, and were stored under dry conditions for SEM analysis in the laboratory. For this study, we focused on samples with particles of the largest size fraction (1–30 μm). Samples from the same geographic location were chosen for analysis in order to allow reconstruction of the dust composition within the atmospheric column. Sampling parameters are summarized in Table 1.

Approximately 22 500 particles in 22 samples were analysed with an environmental scanning electron microscope equipped with backscattered and secondary electron (BSE and SE) detectors and an energy-dispersive X-ray (EDX) detector (FEI ESEM Quanta 200 FEG, Eindhoven, The Netherlands). X-ray spectra were measured by scanning the beam over 80% of the particle ('core mode'). Automated individual particle-analysis was performed with the software package EDAX/AMETEK Genesis 5.231. Measurement conditions were 20 kV acceleration voltage, 'spot size 4' (beam diameter 2–3 nm) and a working distance of approximately 10 mm. Energy-dispersive X-ray spectroscopy was conducted with a Si(Li) detector with subsequent matrix correction by a standardless procedure. The following elements were taken into account: C, O, F, Na, Mg, Al, Si, P, S, Cl, K, Ca, Ti, Cr, Mn, Fe, Co, Ni, Cu and Zn. After automated analysis of a sample every single measured spectrum and associated BSE image of the particle was controlled manually, and analyses with a low signal-to-background ratio and overlapping particles were removed from the data set. A preliminary classification of particles was carried out with the software GROUPP 0.34.4 (Kandler et al., 2011). Detailed classification criteria are given elsewhere (Kandler et al., 2011). Especially for a better discrimination between different (alumo)silicates, all analyses were individually checked afterwards and were 'reclassified' into different subgroups. Groups are defined by the dominance of one or more specific elements (e.g. Ca, Si, SiAl, Cl and CaS groups). An important task is the possible mineralogical interpretation of the different particle groups. For this purpose, all particle analyses were requantified without carbon (in wt.%), and then compared to compositional data from the literature (e.g. mineralogical database on webmineral.com). To describe the chemical composition of particles more precisely, we use elemental ratios (e.g. Si/Al), which are always calculated with analyses given in weight% ('weight ratios'). Especially the silicate groups were separated into subgroups with high and low Fe contents. The boundary was arbitrarily chosen at a Fe content of 5 wt.%.

To characterize the mixing state in more detail, about 1000 particles of sample OZM_08a were analysed manually by spot analysis in the centre of the particle with additional spot analyses on conspicuous features (different contrast in BSE images, particular morphology in SE images). Furthermore, selected particles were characterized by element mapping (C, O, F, Na, Mg, Al, Si, P, S, Cl, K, Ca, Ti and Fe).

Generally, mineral dust particles are not spherical in shape. As a measure for the elongation of the particles, the aspect ratio was calculated with the Genesis software. The aspect ratio AR is described by division of the longest and shortest axis of an ellipse that is fitted to the particle area and is calculated by

$$\mathrm{AR} = \pi L^2/4B, \tag{1}$$

with L the longest projection of the particle outline and B the area of the particle (calculated by the sum of all pixels covered by the particle in the back-scatter electron image). In addition, the average shape factor SF is measured as

$$\mathrm{SF} = 0.07948 P^2/B, \tag{2}$$

with P the periphery length and B the area of the particle. The shape factor is a proxy for the roughness (or smoothness) of the 2D-outline of a particle as observed under the electron microscope. For comparison, the shape factor SF for a sphere is 1.00,

Table 1. Sample name, dust episode, sampling date, start time, number of particles analysed and mean value for the sampling altitude (above ground) for all analysed samples

Sample name	OZM_02a1	OZM_02a3	OZM_03a1	OZM_03a2	OZM_03a3	OZM_03a4	OZM_03a5_2	OZM_03a6_2
Dust episode	Intermediate 1	Intermediate 1	Intermediate 1	Intermediate 1	Intermediate 1	Intermediate 1	Intermediate 1	Intermediate 1
Date	19 May 2006	19 May 2006	20 May 2006	20 May 2006	20 May 2006	20 May 2006	20 May 2006	20 May 2006
Start time, UTC	10:24:34	11:22:29	10:23:17	10:48:15	11:02:05	11:32:39	11:48:06	12:19:10
Particle number	2147	730	527	565	1027	1153	605	583
average altitude	1262 m	1321 m	1762 m	1001 m	1007 m	1016 m	840 m	1775 m
Sample name	OZM_08a1	OZM_08a2	OZM_08a3	OZM_08a4	OZM_08a5	OZM_08a6		
Dust episode	Dust period 2	Dust period 2	Dust period 2	Dust period 2	Dust period 2	Dust period 2		
Date	27 May 2006	27 May 2006	27 May 2006	27 May 2006	27 May 2006	27 May 2006		
Start time, UTC	9:38:12	10:25:25	10:39:07	10:56:51	11:19:26	11:40:40		
Particle number	2082	627	591	627	663	617		
average altitude	2959 m	831 m	834 m	927 m	1419 m	1449 m		
Sample name	OZM_11a1_2	OZM_11a2	OZM_11a3	OZM_11a4	OZM_11a5	OZM_13a2_2	OZM_13a3	OZM_13a4
Dust episode	Dust period 3	Dust period 3	Dust period 3	Dust period 3	Dust period 3	Dust period 3	Dust period 3	Dust period 3
Date	03 June 2006	03 June 2006	03 June 2006	03 June 2006	03 June 2006	05 June 2006	05 June 2006	05 June 2006
Start time, UTC	8:21:00	8:34:37	9:02:32	9:13:14	9:41:05	9:15:21	9:51:45	10:11:01
Particle number	3370	479	1711	618	834	1668	758	365
average altitude	890 m	871 m	2066 m	2104 m	3335 m	2987 m	882 m	2065 m

Table 2. Particle groups with mineralogical interpretation, average particle number abundance, average aspect ratio, and average shape factor (Ca: calcite; CaMg: dolomite), 22347 particles analysed

Particle group	Mineralogical interpretation	Particle number abundance (%)	Particle number abundance (without Cl- and S-bearing particle groups) (%)	Median aspect ratio (mean deviation)	Median shape factor (mean deviation)
Ca (Mg)	Calcite, dolomite	11.6	15.0	1.60 (0.11) Ca: 1.62 (0.11) CaMg: 1.45 (0.11)	1.20 (0.10) Ca: 1.21 (0.09) CaMg: 1.16 (0.08)
Si	Quartz	10.5	13.6	1.55 (0.13)	1.18 (0.13)
SiAl (Fe)	Alumosilicates (kaolinite group, smectite group)	16.8	21.4	1.57 (0.08)	1.24 (0.18)
SiAlK (Fe)	Alumosilicates (illite group, muscovite, K-feldspar)	8.8	11.5	1.56 (0.07)	1.23 (0.09)
SiAlNa (Ca)	Alumosilicates (plagioclase)	2.2	2.9	1.61 (0.07)	1.19 (0.09)
SiAlFeMg (CaK)	Alumosilicates (smectite group, chlorite group)	9.6	12.3	1.57 (0.09)	1.24 (0.15)
SiMg (Al)	Palygorskite/sepiolite	1.7	2.2	1.54 (0.12)	1.21 (0.24)
Fe FeTi Ti	Fe: hematite, goethite FeTi: ilmenite or mixtures Ti: rutile, anatase	1.1	1.5	1.50 (0.13)	1.15 (0.10)
Si(Al) + Ca	Mixtures (alumo)silicates + carbonates	10.0	12.4	1.62 (0.11)	1.33 (0.20)
Si(Al) + S	Mixtures (alumo)silicates + sulphates	8.1	–	1.73 (0.14)	1.29 (0.22)
Cl	(Altered) sodium chloride + mixtures	1.8	–	1.66 (0.11)	1.40 (0.43)
CaS	Gypsum/anhydrite	4.3	–	1.74 (0.43)	1.31 (0.34)
other S	Different sulphates	12.1	–	2.91 (1.11)	1.79 (0.44)
rest	Variable	1.3	1.8	–	–

for a square is 1.27 and for an ellipse with an aspect ratio of 1.5 SF is 1.06. As a measure of dispersion, the mean deviation from the median was calculated for both the aspect ratio AR and the shape factor SF (Table 2).

3. Results

3.1. Definition and characteristics of the different particle groups

In the following chapter, the different particle groups as defined by our classification scheme, their mineralogical interpretation, general abundance, aspect ratio, and shape factor will be described (Table 2). Due to the general low relative humidity in the study area of Northwestern Africa it is assumed that deliquescence of particles only plays a minor role and that the overwhelming fraction of particles were transported in the solid state (but see Kandler et al. (2011) for a detailed discussion of samples from Cape Verde).

3.1.1. Si group. Particles dominated solely by Si are abundant in all samples. Their particle number abundance ranges between approximately 6 and 16%. The mineralogical interpretation of this group is straightforward, and it can be assumed in conjunction with mineralogical studies in Northwestern Africa (Paquet et al., 1984; Avila et al., 1997; Kandler et al., 2007) that the overwhelming portion of these particles consists of the SiO_2 mineral quartz. Silica skeletons of diatoms were only observed occasionally. Most Si group particles show slightly elevated Al contents, pointing to an association of quartz with low amounts of Al-bearing particles (e.g. clay minerals). Element mapping of quartz particles (not shown) occasionally exhibits higher Al and also K, Fe and Mg concentrations at the rim of the particle. This observation can be interpreted as a thin cover of clay mineral particles attached to the quartz grain. The Fe content is generally low indicating that Fe oxides or Fe hydroxides are not preferentially associated with Si-dominated particles.

The median of the aspect ratio of particles of the Si group is 1.55, and the median of the shape factor 1.18. These values are in accordance with the observation of individual Si-rich particles, which mainly show subangular to subrounded forms and only a weak elongation.

3.1.2. SiAl (Fe) group. Particles of the SiAl (Fe) group are characterized by elevated Si and Al contents, whereas Fe may occur as an additional component. This group is the dominant particle group in many samples and reaches particle number percentages of up to 30%. As Si concentrations always exceed

Al concentrations, the presence of the Al_2SiO_5 polymorphs andalusite, kyanite and sillimanite can be ruled out in our samples. The SiAl (Fe) group is interpreted to consist mainly of clay minerals of the kaolinite group (Si/Al weight ratio $\sim$ 1) and the smectite group (Si/Al weight ratio $\sim$ 2.0). As many particles of this group exhibit Si/Al ratios above 2, it seems reasonable to assume significant internal mixing between the above-mentioned clay minerals and a Si-rich phase (e.g. quartz). The overwhelming fraction of particles of this group contains elevated Fe contents. The most probable explanation for this phenomenon is the presence of an additional Fe-rich phase (Fe oxide or Fe hydroxide) in the particles, but some internal mixing between kaolinite and/or smectite and Fe-rich chlorites may also occur. Spot analyses and element mappings of particles of this group often show spots of Fe- or Ti-rich phases (Figs 2b, g and 3b, c), which are interpreted as tiny (<500 nm) grains of Fe oxide (probably hematite) or Fe hydroxide (probably goethite), and Ti oxide (probably anatase, rutile), respectively, which are located at or near the surface of the host particle.

The median of the aspect ratio of particles from the SiAl (Fe) group (about 1.57) is comparable to other silicate groups. The shape factor (median: 1.24) is slightly higher compared to other (alumo)silicate groups which may be explained by the higher abundance of internal mixtures (either mixtures of other phases and clay minerals or mixtures of different clay minerals). These polyphase aggregates consist of numerous small grains, resulting in a higher surface roughness of the particle.

3.2.3. SiAlK (Fe) group. Alumosilicates with significant K concentrations are also relatively abundant in our samples (4–13% by number). Particles of the SiAlK (Fe) group can be subdivided into a subgroup with high K contents and a subgroup with relatively low K contents (arbitrarily chosen boundary at 8 wt.%). Most particles of the high-K subgroup exhibit Si:Al:K weight ratios of approximately 3:1:1 which are indicative for K-feldspar. The particle number abundance of particles with a typical K-feldspar X-ray spectrum is generally low <3% in all samples. The particles of the subgroup with low K content are interpreted to consist mainly of illite and/or muscovite, but it has to be claimed that especially the boundary to the SiAl group is fuzzy. Nevertheless, the ratio between the particle number abundance of 'illite-muscovite' particles (low K particles within the SiAlK (Fe) group) and 'kaolinite-smectite' particles (SiAl group) was calculated and varies between 0.2 and 0.9. SiAlK particles with elevated Fe contents are almost exclusively members of the low-K subgroup, indicating that Fe oxides and Fe hydroxides are preferentially associated with illite-muscovite particles and not with K-feldspar. Fe-dominated phases are observed as spots at or near the particle surface comparable to the observation from particles of the SiAl (Fe) subgroup. Included in the SiAlK (Fe) group are also particles that contain an additional Na component. These rare particles show a Si:Al:(K+Na) weight ratio of 3:1:1, which is again typically for feldspar. Detailed manual single-spot analyses on some of these grains indicate alternating bands of K-rich and Na-rich areas, which point to perthitic or antiperthitic exsolutions in feldspar particles. The median of the aspect ratio of particles of the SiAlK (Fe) is 1.56, the median of the shape factor 1.23.

3.2.4. SiAlNa(Ca) group. The mineralogical interpretation of this group is straightforward because most particles reveal a Si:Al:Na weight ratio of approximately 3:1:1 typical for albitic plagioclase. Much rarer are particles with an additional Ca component, which can be interpreted as Ca-bearing plagioclase or as internal mixtures of albite and calcium carbonates (or nitrates). The particle number percentage of the SiAlNa(Ca) group (between 1 and 4%) is comparable to the particle number abundance of the high-K subgroup of the SiAlK (Fe) group. Analogous to particles of the SiAlK (Fe) group, particles of the SiAlNa(Ca) group exhibit only rarely an additional significant Fe component.

The median of the aspect ratio of particles of the SiAlNa(Ca) group is 1.61 and is comparable to aspect ratios of other groups dominated by alumosilicates. The median of the shape factor from particles of this group is one of the lowest in our samples (1.19), which is in agreement with the observation, that many particles of this group represent single plagioclase grains with subangular forms.

3.2.5. SiAlFeMg(CaK) group. The SiAlFeMg(CaK) group represents a silicatic 'rest group' characterized by elevated Al, Fe and Mg contents, whereas additional Ca or K is only present in some particles. The particle number abundance of this group is more variable compared to other groups (4–17%), probably due to the heterogeneity of particles incorporated within this group. Possible mineralogical phases that fall into this group are for example members of the biotite group, the chlorite group, the amphibole group, or the smectite group, but also internal mixtures between different minerals have to be envisioned. However, the K content in particles of the SiAlFeMg(CaK) group is generally too low for typical biotite compositions, and hence the occurrence of biotite in any significant amount can be excluded. The unequivocal identification of chlorite or amphibole is hampered by their variability in composition. However, (Fe+Mg):Al:Si weight ratios of 9:6:5 which are representative for 'pelitic' chlorites are occasionally observed in our data set, pointing to the presence of chlorite particles at least in minor amounts. The same holds true for particles of the amphibole group, because some analyses match typical compositions of Ca amphiboles quite well. Particles with high Mg contents and relatively high Si:Al ratios (>3) are probably internal mixtures of palygorskite/sepiolite, an alumosilicate (e.g. clay mineral) and a Fe-bearing mineral. However, it must be stated that this group is the least understood in our data set and cannot be easily transferred into mineralogical phases at the moment.

The obvious heterogeneity of this group and the occurrence of internal mixtures are also reflected in a slightly elevated shape factor (median: 1.24). The aspect ratio falls again into a range between 1.50 and 1.60 (median: 1.56).

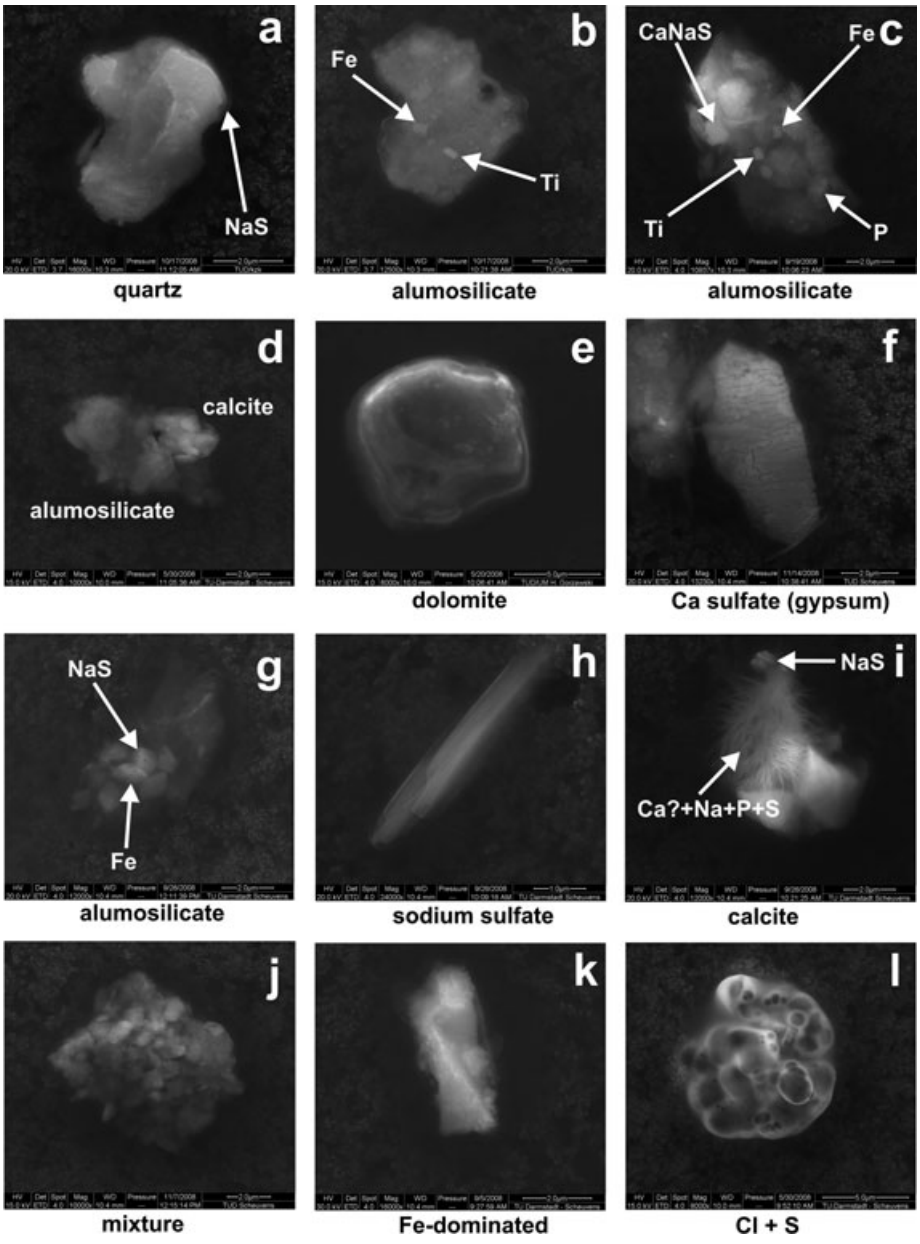

Fig. 2. Secondary electron images of typical particles of airborne mineral dust collected during SAMUM 1. (a) Si-rich particle (quartz) with Na_2SO_4 coating, (b) alumosilicate (clay mineral aggregate) with Fe- and Ti-containing phases, (c) alumosilicate (clay mineral aggregate) with Fe- and Ti-containing grains, CaNa-sulphate, and a P-rich spot, (d) internally mixed particle of alumosilicates and calcite, (e) rounded particle of dolomite with typical low aspect ratio, (f) elongate Ca sulphate (presumably gypsum) showing degassing signs after electron bombardment, (g) alumosilicate particle with attached Na_2SO_4- and Fe-rich particles, (h) needle-like Na_2SO_4 particle, (i) calcite with secondary sulphates/phosphates, (j) complex mixture, (k) Fe-rich particle and (l) ammonium sulphate with relics of a Cl-bearing phase (bubbles are due to degassing under electron bombardment).

3.2.6. SiMg (Al) group. The major portion of particles with elevated Mg and Si contents can be interpreted to represent minerals of the palygorskite/sepiolite group. The particle number percentage of this group is generally very low in our samples (<3%), but some palygorskite/sepiolite particles are at least present in every sample. Many SiMg particles contain an additional Al component, which can best be explained as mixtures of palygorskite/sepiolite with other clay minerals.

Despite the fibrous habit of palygorskite, particles of the SiMg (Al) group have a median aspect ratio of 1.56, which is comparable to the aspect ratio of other silicate groups indicating rounding of palygorskite grains or aggregates. Also SEM images of SiMg

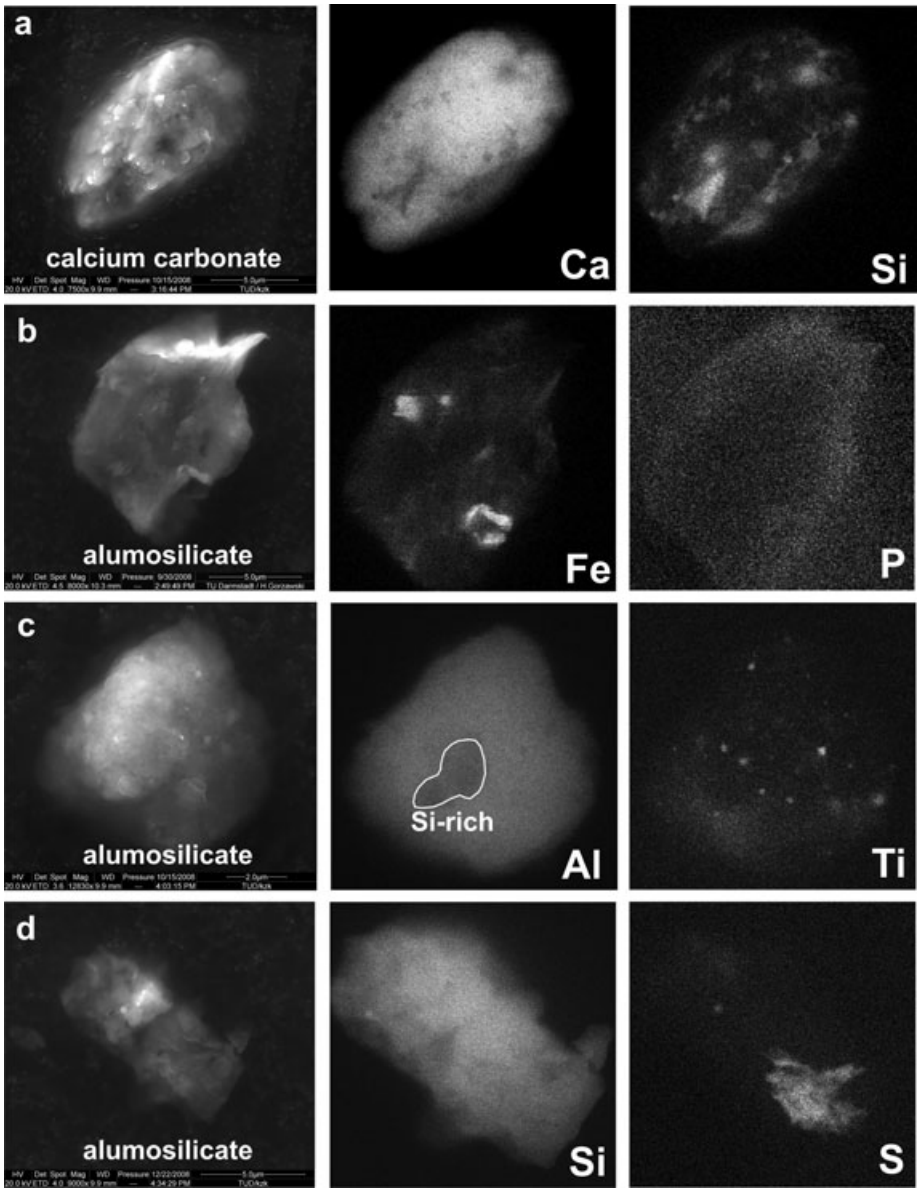

Fig. 3. Secondary electron images (left column) and selected element maps (middle and right column) for different particles of sample OZM_14a3 from 5 June 2006; (a) Ca-rich particle with Si-rich spots pointing to a complex aggregate of calcite and quartz, (b) alumosilicate particle (clay mineral aggregate) with spots of Fe-rich phases and elevated phosphor contents at the rim, (c) alumosilicate particle (clay mineral aggregate) with tiny Ti-rich grains and (d) alumosilicate particle (clay mineral aggregate) with a diffuse area of sulphur enrichment.

(Al) particles are not distinguishable from other silicates. They neither show the fibrous habit typical for palygorskite nor the 'felt-like' structure described by Coudé-Gaussen (1989). The median of the shape factor of particles of the SiMg (Al) group (1.21) falls into the range of the shape factor of other silicate groups.

3.2.7. Ca(Mg) group. Despite the fact that accurate C concentrations are difficult to obtain from our analyses due to the low Z number of carbon and the carbon substrates used for sampling, particles that are dominated either by Ca or by Ca + Mg are interpreted as calcium carbonates and calcium magnesium carbonates, respectively. However, the presence of $Ca(NO_3)_2$ particles cannot be ruled out completely, despite the fact that the spherical shapes typical for $Ca(NO_3)_2$ were not observed (Matsuki et al., 2010).

Calcium carbonates generally occur in two modifications, calcite and aragonite, but it can be assumed that the majority of Ca-dominated particles consists of calcite. Particles of the Ca subgroup are easily discriminated from CaMg-dominated particles which can be correlated with the occurrence of dolomite

[$CaMg(CO_3)_2$]. The particle number abundances of the Ca and CaMg subgroups are rather constant, and fall into a range between 6 and 14% and 0.5 and 3%, respectively. The abundance of Ca-dominated particles is always larger than the abundance of CaMg-dominated particles with a ratio mostly between 4 and 10. It is interesting to note that neither $CaCO_3$ nor $CaMg(CO_3)_2$ particles are associated with significant Fe contents. Spectra of particles that are classified into the Ca(Mg) group only rarely exhibit an additional sulphur peak, excluding significant internal mixing between carbonates and sulphates.

The median of the aspect ratio of particles of the Ca(Mg) group is 1.60. However, a slight difference between particles of the Ca subgroup (calcite) and particles of the CaMg subgroup (dolomite) is observed with higher aspect ratios for calcite particles (median: 1.62) compared to dolomite particles (median: 1.45). The shape factor for particles of the Ca(Mg) group is generally low (median: 1.20) with dolomite particles exhibiting one of the lowest average shape factors of all groups and subgroups (median: 1.16). A typical CaMg particle is shown in Fig. 2e.

3.2.8. CaS group. The mineralogical interpretation of the CaS group is straightforward. Particles which are dominated by calcium and sulphur can be classified as gypsum ($CaSO_4 \cdot 2H_2O$) or anhydrite ($CaSO_4$). After long-time bombardment with the electron beam some particles show cracks pointing to degassing of H_2O indicating the presence of gypsum (Fig. 2f). Ca sulphates represent a minor group in particle number abundance (<10%). It is important to note, that the Ca:S weight ratio of about 1 of the overwhelming part of CaS particles reveals that Ca sulphates are only rarely internally mixed with Ca carbonates. The Ca:S weight ratio of about 1 also rules out a significant contribution of ammonium sulphate to this group which should otherwise lead to an excess of S and consequently lower Ca:S weight ratios.

The median of the aspect ratio of calcium sulphate particles is rather high (median: 1.74) owing to the tabular habit of single crystals of gypsum/anhydrite. The average shape factor of particles of the CaS group is also slightly higher than average (median: 1.31).

3.2.9. Other S. The group of other S-bearing particles contains all particles that are not classified into the CaS group and do not represent mixtures between S-bearing particles and silicates. The 'other S' group can be divided into several subgroups. NaS-bearing particles (Fig. 2h) are interpreted to consist of sulphates such as thenardite (Na_2SO_4) or mirabilite ($Na_2SO_4 \cdot 10H_2O$), whereas CaNaS-bearing particles either represent glauberite [$Na_2Ca(SO_4)_2$] or any mixture between different sodium, calcium and/or calcium sodium sulphates. In addition, mixtures between sodium sulphates and carbonates may contribute to this subgroup. Particles of the NaS and CaNaS subgroups are dominating the group of other S-bearing particles, but a variety of other phases including particles with solely sulphur (probably ammonium sulphate), NaMgS-bearing particles (probably vanthoffite or bloedite) and BaS-bearing particles (barite) are observed. Ammonium sulphates may contribute to all S-bearing subgroups but their rare occurrence as individual particles makes a significant contribution to particles in the here analysed size range (>1 μm) unlikely. A small group of particles contains Ca, Na, P and S as major elements and crystallizes as fibrous aggregates. The mineralogical phase (or phases) which represent this subgroup is unknown, but they probably represent crystallized biofilms. The 'other S' group exhibits the largest variability in particle number percentage (see below), and shows no correlation with the abundance of the CaS group.

Particles of the 'other S' group exhibit the highest average aspect ratios (median: 2.91) and the highest average shape factors (median: 1.79) of all groups. In some samples single particles of the NaS subgroup are characterized by aspect ratios >20 and many particles from the other subgroups are found with AR > 10. Hence an upper limit of the AR value of 5 for Saharan dust samples as observed by Chou et al. (2008) in airborne samples from Niger is not of general validity. However, the interpretation of the origin of particles of this group is not straightforward (see discussion), but many of them may be the result of the advanced processing of primary sea-salt particles and therefore are not 'Saharan dust' in a strict sense. Particles of the Ca + Na + P + S subgroup and the NaS subgroup exhibit very high average shape factors of 1.66 and 2.03, respectively, due to the fibrous and needle-like habit of many of these particles (Fig. 2i).

3.2.10. Fe FeTi Ti group. The Fe FeTi Ti group can be divided into three subgroups. Fe-dominated particles represent the most abundant subgroup, and maximum particle number abundances of 1.5% are observed in some samples. Mineralogical speciation of the Fe-dominated particles is not possible with our analytical approach, but it can be assumed that Fe oxides (e.g. hematite, magnetite) and Fe hydroxides (e.g. goethite) contribute to this subgroup (Fig. 2k). The two other subgroups (FeTi- and Ti-dominated particles) are rare or completely lacking in some samples. Whereas Ti-dominated particles mainly consist of TiO_2 phases such as rutile or anatase, FeTi-dominated particles are interpreted as ilmenite ($FeTiO_3$) or mixtures of Fe oxides/hydroxides with a TiO_2 phase. Additional Ti peaks are also observed in spectra of particles of other groups (mainly alumosilicates), and internal mixing of especially clay minerals and TiO_2 phases is observed in some particles (Fig. 3c). The particle number abundance of the Fe FeTi Ti group never exceeds 2% in our samples.

Particles of this group are characterized by an average aspect ratio of 1.50 (median) with slightly differing median values for the different subgroups (Fe subgroup: 1.48; FeTi subgroup: 1.47; Ti subgroup: 1.51). The average shape factor is low for all subgroups (median: 1.15).

3.2.11. Si(Al) + S group. The Si(Al) + S group compromises particles that are dominated either by SiAl + S or Si + S. The particles of the latter group are mainly interpreted to consist of internal mixtures of quartz and a sulphate. The S-bearing phases of these internal mixtures are either Ca sulphates or one of the

sulphates of the 'other S' group (except barite). Rarely, also mixtures of SiMg-dominated particles of the palygorskite/sepiolite group and different sulphates fall into this subgroup. The particle number percentage of the Si + S subgroup is small compared to the SiAl + S subgroup and never exceeds 2%. Within the SiAl + S subgroup all internal mixtures of any alumosilicate (e.g. different clay minerals, feldspar, chlorite) and any sulphate are summarized. Again the S-bearing portion of the particle is assumed to consist of members of the CaS and/or the 'other S' group (see detailed discussion later). Observations on single particles of this group show different types of internal mixtures. Most abundant are alumosilicate aggregates that show irregular spots (Fig. 3d) or small euhedral grains of S-bearing phases (Figs 2c, d and g). More rarely, distinctive rims around silicate and alumosilicate particles are observed in SE and BSE images. These rims show elevated S contents (detected by spot analysis) and are interpreted as coatings or partial coatings of a sulphur-bearing phase (mainly sodium sulphates) on quartz or alumosilicates (Fig. 2a). In a few cases, the contrast between particle and coating was high enough to measure the thickness of the coating which was determined to range between 150 and 300 nm.

In all samples, the ratio of the particle number percentage of the Si group and the Si + S subgroup is lower than the ratio of the particle number percentage of the sum of all alumosilicate groups divided by particle number percentage of the SiAl + S subgroup. This relationship points to a preferential internal mixing of alumosilicates and sulphates relative to quartz and sulphates. The particle number abundance of the SiAl + S subgroup is highly variable and falls into a range between 0 and 20%. This variability in abundance will be described below.

Generally, the median of the aspect ratio and the median of the shape factor of particle groups that completely represent internal mixtures [e.g. Si(Al) + S group, Si(Al) + Ca group] are higher than average. The median of the aspect ratio of particles of the Si(Al) + S group is 1.73, the median of the shape factor 1.29. The slightly increased AR and SF values are explained by the aggregation of different phases, leading to an elevated elongation and to rougher surfaces of these irregular aggregates. The increased AR and SF values also underline the finding that sulphur coatings, which should result in smoother surfaces and consequently lower SF values are comparatively rare in our samples.

3.2.12. Si(Al) + Ca group. As the Si(Al) + S group, the Si(Al) + Ca group can be split into 2 subgroups, the SiAl + Ca subgroup and the Si + Ca subgroup, respectively. The particle number abundance of the latter is small and does not exceed 1%. As wollastonite ($CaSiO_3$) is rare in nature and the Ca:Si ratio is highly variable in particles of the Si + Ca subgroup, it is very probable that particles of this subgroup consist of internal mixtures of a Si-rich phase (e.g. quartz) and a Ca-rich phase (e.g. calcite; see Fig. 3a). Owing to its high particle number percentage of up to 16%, the SiAl + Ca subgroup is much more important than the Si + Ca subgroup. The good correlation between the particle number abundance of the Ca(Mg) group and the SiAl + Ca subgroup indicates that the latter mainly consists of internal mixtures of different alumosilicates and Ca(Mg) carbonates (Fig. 2d). As the Na and K contents in particles of this subgroup are generally low and Si:Al weight ratios around 3 are only rarely encountered, a major contribution of feldspar minerals to particles of the SiAl + Ca subgroup can be excluded. The most reasonable explanation for the composition of many particles of this subgroup is internal mixing of 'non-feldspar' alumosilicates (e.g. clay minerals) with Ca carbonates (e.g. calcite). The Fe contents in many particles of the SiAl + Ca subgroup are comparatively high pointing to an additional contribution of Fe oxides/hydroxides. The participation of other Ca-bearing minerals (e.g. amphiboles, pyroxenes) cannot be ruled out completely, but should be of minor importance.

The conclusion that particles of the Si(Al) + Ca group are mainly represented by internal mixtures is corroborated by a comparatively high aspect ratio (median: 1.62) and an elevated shape factor (median: 1.33). The measured shape parameters point to elongate and irregular aggregates of carbonates and alumosilicates. The latter were also directly observed in the electron microscope (Fig. 2d).

3.2.13. Cl group. Particles with significant chlorine content mainly belong to three subgroups. First, particles containing Na and Cl are interpreted as sodium chloride particles (Na/Cl weight ratios between 0.5 and 1.5). Particles that contain only Cl as their major component are characterized by slightly elevated sulphur concentrations and most probably represent altered sodium chloride particles. The third group comprises different internal mixtures of NaCl- or Cl-bearing particles with (alumo)silicates, and more rarely with sulphates (see Fig. 2l). The particle number abundance of this latter group is generally low and varies from 0 to a maximum of 8.3%.

The median of the aspect ratio and the median of the shape factor of particles of the Cl group is 1.66 and 1.41, respectively. Unaltered sodium chloride particles only occur in samples from 19 and 20 May. They are characterized by a comparatively lower average aspect ratio of 1.50 and a lower average shape factor of 1.21 due to the cubic symmetry and the isometric habit of sodium chloride. Higher aspect ratios are recorded for internal mixtures of Cl-bearing and S-bearing particles (median: 1.87).

3.2.14. Rest group. The so-called rest group contains all particles that do not fall into any of the other above-described groups. Hence, it represents a vast mixture of different particles. The rest group includes a whole range of particles from particles dominated by a single element to particles, which represent complex internal mixtures. Some of the subgroups with their dominant elements and a possible mineralogical interpretation are given in Table 3. Included within the rest group are Al-dominated particles, different secondary nitrates and hydroxides, the P-bearing mineral apatite [$Ca_5(PO_4)_3(F,Cl,OH)$], and the Ti-rich mineral sphene ($CaTiSiO_5$). The particles of the

Table 3. Mineralogical interpretation for particles of the 'rest' group

Particle subgroup	Mineralogical interpretation
Al	Al oxides (corundum) or Al hydroxides (diaspore, boehmite, gibbsite)
Na	Na nitrate or Na carbonate
K	K nitrate, K carbonate or K hydroxide
Mg	Mg oxide/hydroxide or Mg carbonate
CaP	Apatite
CaSiTi	Sphene
Mixture	–
CuZn	Steel (partially artefacts?)

'mixture' subgroup are mainly dominated by Si, but contain different other elements in variable amounts and therefore are not classified in any silicate group. The particle number percentage of the rest group is low with a maximum of 2.3%.

3.2. *Relative abundance of particle groups*

Our study reveals that airborne samples from Morocco are dominated by SiAl-, Si-, Ca(Mg)- and S-bearing particles (Table 2). These chemical categories can be transferred into the mineralogical components of clay mineral mixtures, quartz, carbonates, different sulphates, and mixtures between carbonates and alumosilicates as well as between sulphates and alumosilicates. Feldspar minerals, palygorskite, Cl-bearing components (including sodium chloride) and Fe- and Ti-bearing minerals only occur in minor amounts.

Excluding all Cl- and S-bearing groups and normalizing again to 100% (Fig. 4), an extremely homogeneous compositional data set emerges. This homogeneity in particle number abundance of the different particle groups is observed between individual samples, between single sampling days, and between the different episodes. Also no compositional trends with respect to altitude are discernable, regardless if one considers the complete data set or the partial data set where Cl- and S-bearing groups are neglected.

However, significant variations in particle number abundance are observed for the groups of chlorides and sulphates, respectively (Fig. 5). Whereas chlorides occur in minor amounts on 19 May, 20 May (intermediate period 1) and 3 June (dust episode 3), they are virtually absent on 27 May, (dust episode 2) and 5 June (episode 3). Furthermore, the chloride component on 19 May and 20 May (intermediate period 1) is represented by sodium chloride and mixtures between sodium chloride and alumosilicates. In contrast, samples of 3 June (dust episode 3) only contain pure chlorine-bearing particles (without Na or K component), pointing to significant aging and loss of alkali metals. Mixing between Cl-bearing particles and alumosilicates

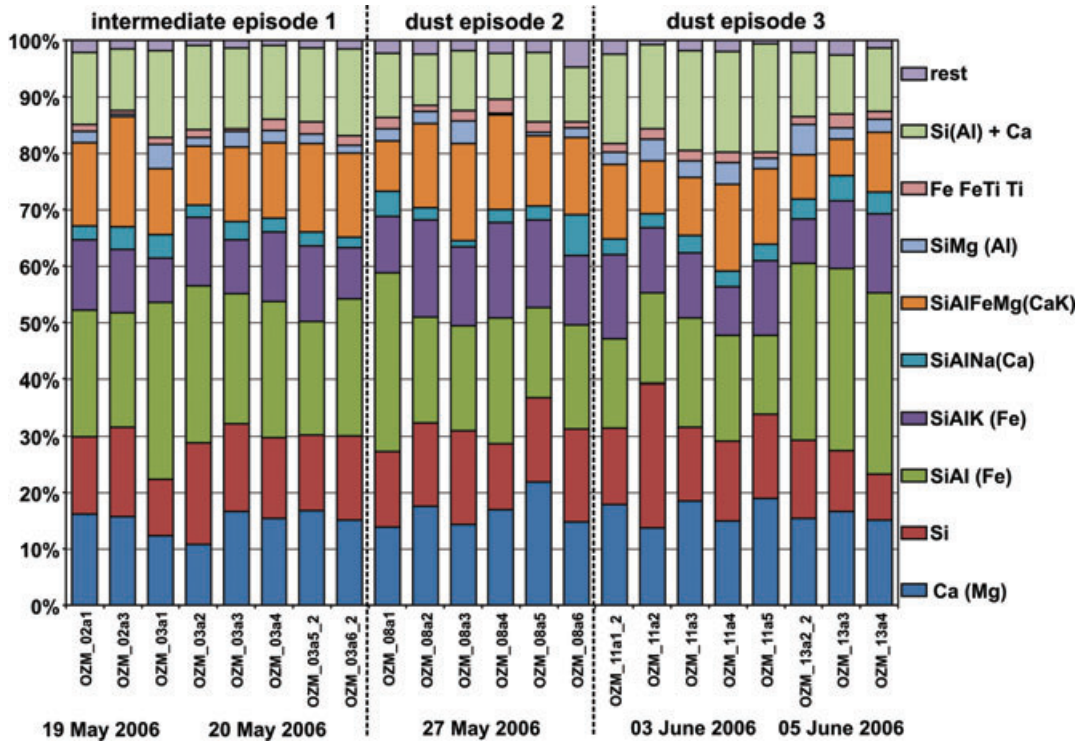

Fig. 4. Chemical composition (relative number abundance of different particle groups) of airborne dust samples collected in May and June 2006 in southern Morocco neglecting all Cl- and S-bearing particle groups (sample names according to Table 1).

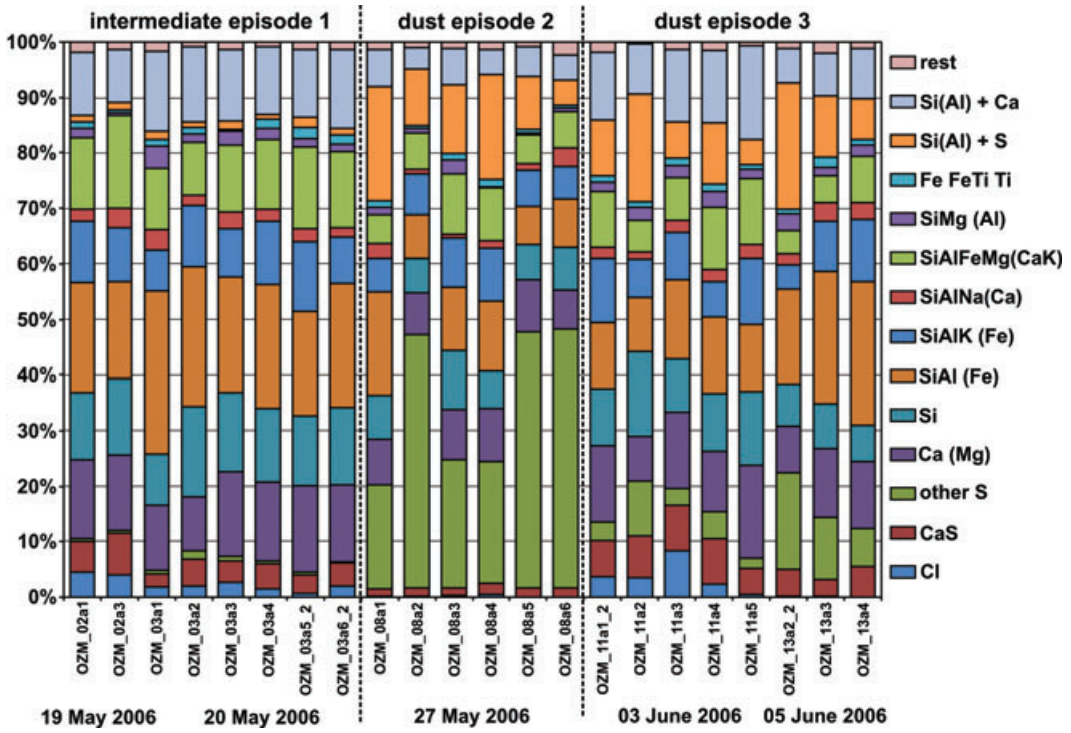

Fig. 5. Chemical composition (relative number abundance of different particle groups) of airborne dust samples collected in May and June 2006 in southern Morocco (sample names according to Table 1).

is less frequent compared to days 19 and 20 May (intermediate period 1).

The major compositional variability between single sampling days is due to different number abundances of S-bearing particles. Especially, the particle number abundance of the 'other S' group exhibits large differences. Particles of the 'other S' group are almost absent in the first intermediate period (19 and 20 May), represent a major group during dust episode 2 (27 May), and occur in minor amounts during dust episode 3 (3 and 5 June). Neglecting samples OZM_08a2, OZM_08a5, and OZM_08a6, which show extremely high particle number abundances of the 'other S' group (approximately 50%), a good linear correlation between the group of mixtures between silicates and sulphates and the sum of the CaS group and the 'other S' group is observed. Hence, it can be concluded that both groups are involved in internal mixing of S-bearing particles and silicates. This conclusion is also corroborated by a closer examination of the EDX analyses of individual particles, where both mixtures of CaS- with AlSi-bearing particles and mixtures of Na(Mg)S-bearing particles with AlSi-containing particles can be recognized. However, the correlation between the particle number abundance of the SiAl + S subgroup and the 'other S' group is higher than the correlation between the particle number percentage of the SiAl + S subgroup and the CaS group. This leads to the conclusion that the sulphur component in internal mixtures of alumosilicates and sulphates mainly stems from other sulphates than Ca sulphate.

An interesting phenomenon is the inverse correlation of the 'other S' group and the group of chlorides. The following cases are observed: (a) samples with elevated sodium chloride contents contain only a few particles of the 'other S' group (sample days 19 and 20 May), (b) samples with Cl-bearing particles (without Na or K) also show elevated abundances of the 'other S' group, and (c) samples with high particle number abundances of the 'other S' group are almost free of Cl-bearing particles (sample days 27 May and 5 June). Furthermore, the particle number percentage of the Cl group and the CaS group also exhibit a linear correlation, pointing to partial formation of gypsum/anhydrite by the conversion of sodium chloride. In contrast, the correlation of the Ca group (carbonates) and the CaS group (gypsum/anhydrite) is low, showing that conversion of carbonates to gypsum/anhydrite is not an important process in our samples. Significant internal mixing between carbonates and Ca sulphates is also excluded by a closer examination of the composition of particles of the CaS and the Ca(Mg) group, respectively (see above).

4. Discussion

4.1. Chemistry and mineralogy

Our compositional data set of the large grain-size fraction (geometric diameters between about 1 and 30 μm) of airborne samples taken over Morocco in May and June 2006 is a

supplement to earlier mineralogical (Alastuey et al., 2005; Avila et al., 1997; Paquet et al., 1984; Kandler et al., 2009) and individual-particle EDX/SEM studies (Kandler et al., 2007, 2009) of mineral dusts from northwestern Africa. The average composition of our samples in particle number percentage is 39% alumosilicates, 12% calcium carbonates, 12% secondary sulphates ('other sulphates'), 11% quartz, 10% mixtures between silicates and Ca carbonates, 8% mixtures between silicates and sulphates, 4% Ca sulphates, 4% Cl-bearing particles, Fe oxides/hydroxides and other particles.

The major variability in particle number abundance is encountered for Cl- and S-bearing particles. These differences are interpreted to represent different degrees of aging of sodium chloride. In intermediate phase 1, practically unaltered sodium chloride is observed. Meteorological conditions at these days (19 and 20 May) were dominated by a surface high over the eastern Atlas and intruding air masses from eastern and central Algeria (Knippertz et al., 2009). However, back trajectories can partly be traced back to the southern Mediterranean Sea and hence a maritime origin for the sodium chloride particles cannot be ruled out. During dust episode 2, the highest particle number abundance of sulphates is observed, and chloride-bearing particles are extremely rare. The sampling day (27 May) marks the end of the dust episode and is characterized by a cut-off low with unsettled weather conditions and rain fall on 26 May (Knippertz et al., 2009). The distribution of back trajectories is complicated, but intrusions of air parcels from the Mediterranean Sea can be inferred. It is proposed that sodium chloride particles that are transported from the Mediterranean Sea are completely converted to sulphates under the comparatively humid conditions of that period. The high abundance of 'secondary' sulphates (mainly Na and CaNa sulphates) may additionally have benefitted from elevated SO_2 contents associated with polluted air masses from the Mediterranean region. Unfortunately there are no SO_2 measurements to underline this idea. The elevated amount of secondary sulphates on 27 May may also imply a higher abundance of cloud condensation nuclei for this sampling day, as secondary sulphates are the dominating soluble aerosol component. Dust episode 3 is characterized by internal and external mixing of Cl- and S-bearing particles and lack of 'fresh' sodium chloride particles. Hence, the composition of samples from dust episode 3 is intermediate between samples from intermediate episode 1 and dust episode 2 with a higher degree of aging on 05 June compared to 03 June. Meteorological conditions are dominated by a cut-off low in the Atlas region and a lee cyclone shifting towards east, accompanied by a cold surge from the Mediterranean and days with high dust loads (Knippertz et al., 2009). Calculation of back trajectories points to linearly arranged dust sources from central Algeria to Tunisia (Knippertz et al., 2009). Input of particles that were transported from the Mediterranean region should be minor during dust episode 3. The provenance of the Cl-bearing particles in samples from 03 June is unclear. They may either have originated over the Mediterranean Sea representing aged sea salt and/or may have uplifted from sediments in the zone of chotts in northern Algeria and Tunisia. This area is characterized by powdery soils that besides abundant calcite also contain calcium sulphates and sodium chloride (Rognon et al., 1989). Taken together, source identification for particles containing elevated Cl contents is difficult and they could have both a maritime (Mediterranean) and terrestrial (zone of chotts) source. Significant compositional differences (e.g. in Mg, K or Ca contents) between chlorine-bearing particles from different samples, sample days, or dust episodes are not recognized.

The main fraction of secondary phases is represented by different Na- and NaCa-bearing sulphates (occasionally with an additional Mg component). As particles that contain solely Na are relatively scarce, it is suggested that Na nitrates (the low-Z element N was not considered in our analysis) only represent a minor component. The presence of $Ca(NO_3)_2$ cannot be ruled out, because SEM/EDX analysis is unable to differentiate between $CaCO_3$ and $Ca(NO_3)_2$, but as stated above the spherical particle type typical for $Ca(NO_3)_2$ is not observed in our samples. Particles solely dominated by sulphur as for example ammoniumsulphate $[(NH_4)_2SO_4]$ are also very rare in our samples. They often contain an additional Cl component pointing to aging of sodium chloride particles (Fig. 2l). However, ammonium sulphate particles are an important constituent of the fine grain size fraction (<500 nm) as shown by Kandler et al. (2009).

Neglecting the S- and Cl-bearing particles which are mostly not Saharan dust sensu strictu, but partly have an anthropogenic or maritime source, an average composition of 53% alumosilicates, 16% calcium carbonates, 15% quartz, 13% mixtures between silicates and Ca carbonates and 3% Fe oxides/hydroxides and other particles (in particle number abundance) is calculated for all samples. This composition is very similar to the composition of dust samples from Tenerife from the summer of 2005, which were mainly derived from central Algerian sources (Kandler et al., 2007), and from ground-based samples at Tinfou (southern Morocco) from May and June 2006 (Kandler et al., 2009). Our calculated composition is also broadly in accordance with mineralogical data obtained from X-ray diffraction analysis of ground-based samples from Morocco (Kandler et al., 2009) and Tenerife (Alastuey et al., 2005), and 'red rain' samples from northeastern Spain (Avila et al., 1997) and southeast Italy (Blanco et al., 2003), where back-trajectory analysis also point to source regions in Algeria and Morocco. Samples of the above listed mineralogical studies mention quartz, clay minerals (illite > kaolinite) and carbonates (calcite > dolomite) as the major constituents (amount in weight%), and palygorskite and feldspar as additional important components (Avila et al., 1997; Alastuey et al., 2005). Especially elevated calcite contents and the occurrence of palygorskite were claimed as source markers for mineral dusts from Western Sahara, Morocco, northern Algeria and Tunisia (Paquet et al., 1984; Schütz and Sebert, 1987; Coudé-Gaussen et al., 1987; Coudé-Gaussen, 1989; Moreno et al., 2006; Kandler et al., 2007). Also the mineralogical soil

maps of Claquin et al. (1999) and Desboeufs and Cautenet (2005) as well as a modified soil map of the Harmonized World Soil Database (Fig. 1; FAO/IIASA/ISRIC/ISSCAS/JRC, 2009) show an enrichment of calcite in northern regions of northern Africa. The idea of compositional fingerprints for specific source areas in northern Africa is clearly corroborated by our individual-particle analysis, which also reveals elevated contents of Ca and CaMg carbonates and the occurrence of palygorskite in the studied samples. Mineral dust uplifted in the northwestern part of northern Africa (Morocco, northern Algeria and Tunisia) is mainly transported to the north towards and across the Mediterranean (Engelstaedter et al., 2006; Müller et al., 2009) or more rarely across the African coast in a southwesterly direction and may then be subjected to long-range transport across the Atlantic ocean (Stuut et al., 2005). Whereas calcite may be partly converted to sulphate or nitrate during transport (Krueger et al., 2004; Desboeufs and Cautenet, 2005; Matsuki et al., 2010), the detection of palygorskite in far-travelled dust samples point to an origin in northwestern African source regions (Molinaroli, 1996; see Bout-Roumazeilles, 2007; Verrecchia and Le Coustumer, 1996 for a compilation of palygorskite occurrences in northern African sediments).

Despite the fact that the ratio of the particle number percentage of the SiAl (Fe) and the SiAlK (Fe) groups is only a rough approximation of the ratio of illite plus muscovite to kaolinite plus smectite, the calculated value below 1 is significantly lower than reported illite/kaolinite ratios based on XRD analysis of samples from northwestern Africa (Paquet et al., 1984; Avila et al., 1997; Caquineau et al., 2002; Kandler et al., 2009). This discrepancy can be explained by a significant amount of particles of the smectite group in our samples, which are included together with kaolinite within the SiAl (+Fe) group. Elevated contents of smectite group minerals were also reported for red rain samples from Spain which originated in central Algeria (Avila et al., 1997), but were only detected in trace amounts by Paquet et al. (1984).

In contrast to other studies (Dentener et al., 1996; Alastuey et al., 2005) internal mixing between Ca(Mg) carbonates and sulphates (e.g. coatings of sulphate on carbonate particles) or conversion of carbonates to sulphates is only of minor importance in our samples. The lack of transformation of Ca carbonates to Ca sulphates may be due to the comparatively short transport distances of our samples (Desboeufs and Cautenet, 2005 for a detailed discussion of the prerequisites for calcite to Ca sulphate conversion). The lack of correlation between Ca sulphates (gypsum/anhydrite) and secondary sulphates points to a different origin for the major fraction of particles of both groups. It is suggested that Ca sulphate particles are at least partly of natural origin probably stemming from the zone of chotts in northern Algeria and Tunisia (Prospero et al., 2002 for a detailed description), whereas the secondary sulphates are of anthropogenic origin (air-pollution particles) and/or the result of conversion of sea-salt particles from the Mediterranean basin by the reaction with H_2SO_4 and/or SO_2 (Zhuang et al., 1999). It is interesting to note, that samples from dust episode 2 and dust episode 3 exhibit a comparatively large fraction of internal mixtures of alumosilicates and sulphates pointing to a faster coalescence process after dust entrainment in contrast to the behavior of the carbonate particles (see above). This observation points to a higher nucleation rate (either from the liquid or gaseous phase) of sulphates on alumosilicates (e.g. clay minerals) compared to carbonates. Important factors for heterogeneous sulphate formation are for example the concentration of SO_2, the uptake coefficient of gases, the exact composition of the host particle, and the surface area of the particle. The preferential internal mixing of sulphates and alumosilicates in our study is probably mainly due to the increased surface area of the clay mineral aggregates compared to the rounded calcite particles, but other factors have to be taken into account. Matsuki et al. (2010) in a study of airborne samples from Niger showed that especially Ca-rich particles are affected by a conversion to $Ca(NO_3)_2$. This conversion is not observed in our samples. It is suggested that the observed differences (significant internal mixing of alumosilicates and sulphates in our study; conversion of Ca carbonates to Ca nitrate in Niger) are mainly the result of different gaseous concentrations (SO_2, NO_2) in the atmosphere during the formation of the internally mixed particles. Sulphates occur either as small grains attached to alumosilicates or as coatings, but in contrast to results provided by Kandler et al. (2007) from individual-particle analysis of samples from Tenerife, the latter does not seem to be dominant. The observed difference in the type of internal mixing (neo-formation of sulphate grains in this study vs. coatings in Tenerife) is probably due to variations in relative humidity which in turn leads to different dominant formation processes of internal mixtures of alumosilicates and sulphates. Our direct measurements of coating thicknesses of 150–300 nm are higher than the calculated values of 20–60 nm of Kandler et al. (2007, 2009), but this difference can be explained by smearing out of the sulphur coating during impaction on the carbon substrate.

The presence and abundance of iron oxides/hydroxides (and black carbon) mainly determines the absorption of light in mineral dust (Alfaro et al., 2004; Lafon et al., 2006). Almost pure Fe particles are relatively scarce ($<1.5\%$ in particle number abundance) in our airborne samples from Morocco and less abundant than in samples from more southerly source areas (Chou et al., 2008). However, in accordance with findings of Kandler et al. (2007) an iron component is ubiquitously detected in alumosilicate particles and only to a much lesser extent in quartz, carbonate, and sulphate particles. Especially detailed spot analysis and element mappings of alumosilicate particles (mainly clay mineral aggregates) show that Fe oxides/hydroxides are present in the form of small grains ('spots') at or near the surface of the particle. Comparable observations were made for mixtures of alumosilicates and Ti-rich particles (TiO_2: rutile, anatase), which also occur as tiny spots at or near the surface (Figs 2b and

3c). Owing to their high abundance, the absorption behaviour of these mixed alumosilicate/Fe (hydr)oxide and/or Ti oxide particles is crucial for the determination of the absorption of the bulk sample (Sokolik and Toon, 1999), and was analysed by optical modelling (Lafon et al., 2006). However, the exact distribution of iron oxides/hydroxides and clay minerals in such mixed aggregates is currently unknown and needs further investigation.

Fe is not only present in the form of Fe oxides/hydroxides but also incorporated into the crystal lattice of many alumosilicates. Hence, the fraction of soluble Fe that is available after deposition in marine or terrestrial ecosystems as a nutrient is difficult to estimate with our analytical approach. Phosphorus, the second important nutrient for marine and terrestrial ecosystems occurs in three different speciations. First, it is incorporated into the crystal lattice of apatite, second, it occurs as a component of fibrous aggregates together with Ca, Na and S (probably former biofilms), and third, a phosphorus-bearing phase was sporadically observed as coatings on different alumosilicate particles (Fig. 3b). The solubility of the three different speciations in our samples is unknown, but it can be expected that the solubility of apatite is generally low (Prospero et al., 1996), and that apatite particles are less soluble than the two other phosphorus-containing phases. Hence, probably only a fraction of the total phosphorus content in our samples will be available as a nutrient in marine or terrestrial ecosystems. Furthermore, it has to be claimed that the particle number abundance of particles with elevated P contents is generally very low in our samples.

4.2. Vertical distribution and temporal evolution of dust composition

The knowledge of the vertical distribution of the composition of mineral dust is essential for the estimation of effects of mineral dust on the radiation balance and also important for a reliable retrieval of aerosol optical depths from satellite data. Comparable to the approach of Matsuki et al. (2010) for airborne samples from Niger, this paper presents compositional data based on individual-particle analysis for an 'in-situ' atmospheric column for one intermediate and two dust episodes. Our data set exhibits a very homogeneous chemical composition for the different sampling days independent of sampling altitude (800–3300 m above ground). A notable exception is the lower abundance of Cl-bearing particles in the sample with the highest altitude on 3 June 2006. The latter is in agreement with observations of Kandler et al. (2009) (see their fig. 18). However, the compositional contrast between Ca-rich samples in lower altitudes and Ca-poor samples in higher altitudes for that day (Kandler et al., 2009) could not be reproduced by our analysis. This apparent contradiction can be resolved when considering the different particle sizes that were analysed in both studies. Whereas Kandler et al. (2009) provide compositional data for particles between 1 and 2.5 μm, particles from this study were analysed in a much larger size range (between 1 and 30 μm). This in turn shows, that the compositional difference observed by Kandler et al. (2009) is largely restricted to smaller particle sizes, and that the reported atmospheric stratification on this day (e.g. Petzold et al., 2009; Weinzierl et al., 2009) is mainly due to the intrusion of a low-altitude dust layer with comparatively small particles sizes from an Algerian source region in the east.

The homogeneity in dust composition in the atmospheric column is already achieved during the morning hours of each sampling day, when the new mixed layer still develops and raises to elevated heights of about 4000 m (Heese et al., 2009; Knippertz et al., 2009; Tesche et al., 2009). However, the compositional homogeneity is not only observable as function of altitude on single sampling days. Neglecting S- and Cl-bearing particles, which are mainly the result of 'non-Saharan emission' (marine influence, presence of anthropogenic SO_2/H_2SO_4 in the atmosphere), also the temporal compositional variation of our airborne samples is very limited, and is also independent of the absence or presence of a dust episode in the sampling period. The compositional homogeneity is rather surprising, because different dust source areas in Morocco, Algeria and Tunisia were activated during the campaign (see also Kandler et al., 2009). Generally, dust samples of 19 and 20 May and 27 May with source regions in central and western Algeria (Knippertz et al., 2009) should have lower calcite contents as dust samples of dust period 3 from more northerly source regions (Avila et al., 1997; Paquet et al., 1984). The compositional homogeneity in our samples implies fast mixing with a regional persistent background aerosol after dust entrainment and/or mixing of the transported mineral dust with dust locally uplifted in the surroundings of the sampling site at Ouarzazate (Knippertz et al., 2007, 2009). Based on TSP measurements, the presence of a persistent background dust aerosol in this area was already shown by Kandler et al. (2009). The occurrence of well-mixed dust layers on most days during the sampling period in May and June 2006 was also described by Weinzierl et al. (2009) on basis of the analysis of dust number size distributions. Additionally, a fast achievement of compositional homogeneity was reported by Chou et al. (2008) from airborne dust samples taken over Niger. However, our study also shows that typical compositional characteristics of the larger source area of northwestern Africa (e.g. elevated carbonate contents, occurrence of palygorskite, low content of Fe oxides/hydroxides) are still recognizable in our samples.

4.3. Particle shape

The aspect ratio AR and the shape factor SF were determined for about 22 500 particles and for all compositional groups separately (Table 2). The median of the aspect ratio of particles of the different silicate groups (quartz, feldspar group, clay minerals of the kaolinite, illite, smectite and chlorite groups), of particles of the Fe, FeTi, and Ti subgroups (e.g. goethite, hematite, ilmenite, rutile and anatase), and of particles of the Ca(Mg) group (calcite, dolomite) fall into a range between 1.50 and 1.61. These

values are slightly higher than values reported by Matsuki et al. (2010) (median = 1.4), and slightly lower than data published by Kandler et al. (2007) (median = 1.64), Chou et al. (2008) (median = 1.7) and Kandler et al. (2009) (median = 1.6). They are significantly lower than values reported by Reid et al. (2003) (median = 1.9) for particles subjected to long-range transport from northern Africa to the Caribbean region. Despite the limited data set, a trend with increasing average aspect ratios towards higher transport distances of mineral dust may be inferred.

Lowest aspect ratios are found for sodium chloride (1.50), dolomite (1.42) and Fe- and Ti-dominated particles (1.50). In accordance with the analysis of Kandler et al. (2009), highest aspect ratios are revealed for the group of Ca sulphates (1.74) and the group of 'other sulphates' (2.91). Whereas the high elongation of Ca sulphate particles is due to their needle-like habit, the high aspect ratios of the secondary sulphates are partly the result of the crystallization of solute droplets (Kandler et al., 2009). Our data set also shows that internal mixtures of carbonates and silicates, sulphates and silicates and chlorides and silicates exhibit slightly higher aspect ratios than particles of groups that are (at least partially) represented by a single phase. It may be concluded that a higher extent of internal mixing in dust samples results in higher average aspect ratios, perhaps also partially explaining the higher aspect ratios of 1.9 provided by Reid et al. (2003) from the Caribbean region. An average aspect ratio between 1.50 and 1.61 (expressed as median) is in accordance with results from analysis of lidar and sun-photometer measurements which reveal that aspect ratios of 1.5 and higher are typical for particles of desert dust plumes (Dubovik et al., 2006; Otto et al., 2009). Dust particles are mainly not spherical or ellipsoid in shape, but exhibit non-elliptical outlines in the electron microscope ranging from smooth to highly irregular. This is corroborated by our calculation of the average shape factor for the different groups. Whereas the shape factor of an ellipse with an aspect ratio of 1.5 is 1.06, the median shape factors of silicates, carbonates and Fe- and Ti-dominated particles lie in the range between 1.15 and 1.25 (Fig. 6 and Table 2). However, these values are still below the shape factor of a square (SF = 1.27), providing evidence for the comparatively smooth outline of most particles. Hence, a calculation of volume, mass and/or refractive index based on the assumption of ellipsoid particle shapes is justified for mineral dust (Kandler et al., 2007, 2009, 2011; Lieke, 2011). Higher aspect ratios of ellipses are correlated with higher shape factors (Fig. 6). Elevated shape factors with respect to the general trend are observed for Cl-bearing particles and for mixtures of silicates and carbonates (Si(Al) + Ca group; Fig. 6). Higher shape factors for Cl-bearing particles are the result of the dominance of particles that contain only Cl. These particles are most probably the product of aging and alteration of NaCl particles, which generates particles with lobate outlines. The increased shape factor of the internal mixtures of silicates and carbonates are explained by the irregular surface of these aggregates which also can be recognized by direct observation in the electron microscope (Fig. 2d). Based on our data set, we also calculated the median of the shape factor and aspect ratio for different size classes (>7 μm, 4–7 μm, 1–4 μm geometric diameter) regardless of composition. Both, the lowest average shape factor (SF = 1.21 ± 0.24) and the lowest average aspect ratio (AR = 1.55 ± 0.29) is found for particle sizes between 4 and 7 μm, whereas shape factors and aspect ratios for larger

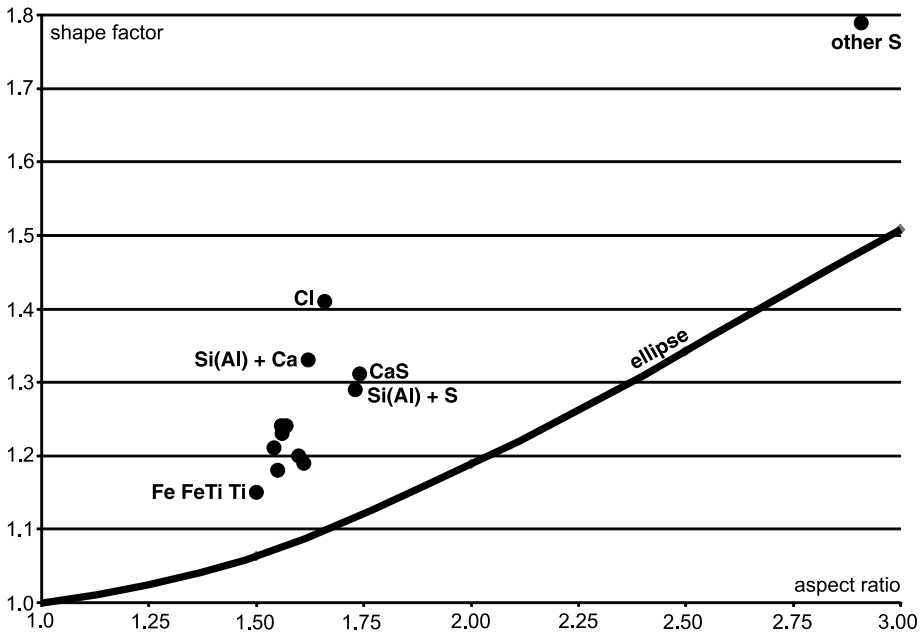

Fig. 6. Median aspect ratio (AR) versus median shape factor (SF); the AR/SF ratio for an ellipse is shown as line; particle groups as in text.

and smaller size classes are slightly higher (>7 μm: SF = 1.35 $\pm$ 0.44, AR = 1.62 $\pm$ 0.33; 1–4 μm: SF = 1.27 $\pm$ 0.49, AR = 1.75 $\pm$ 0.89). However, the large values for the mean deviation of the median values show the heterogeneous population of particles summarized under the different size classes. Hence, a clear tendency of the aspect ratio or shape factor depending on particle size cannot be demonstrated with our data set.

5. Conclusions

During the course of the first phase of the Saharan Mineral Dust Experiment (SAMUM 1) in May and June 2006, airborne dust samples were collected over Ouarzazate and Zagora (southern Morocco) in different altitudes. Individual particle-analysis of about 22 500 particles in 22 samples provides information about the compositional variability in time and height. The following conclusions can be drawn.

1. The major compositional differences between single sampling days are due to variable abundances of Cl- and S-bearing particles. Three different situations can be distinguished: (a) sampling days with comparatively small amounts of 'fresh' sodium chloride particles and very low abundances of secondary sulphates, (b) sampling days with substantial mixing of Cl- and S-bearing particles, and (c) sampling days with high concentration of secondary sulphate particles. This variable degree of aging is most probably due to external parameters such as humidity and/or SO_2 content of the air masses. The occurrence of abundant secondary sulphates also shows that in freshly emitted mineral dust subjected to short- to medium-range transport the fraction of secondary phases may be high, even for large particles.

2. The composition of desert dust in sensu strictu (i.e. disregarding marine and/or anthropogenic components) is remarkably constant. This compositional homogeneity is observed as function of altitude as well as function of time. As different source regions were activated during the different dust episodes, fast mixing of dust after uplift from different emission spots with a persistent regional dust background aerosol is implied. However, it is important to note that the newly generated mixed dust still exhibits typical compositional features (source tracers) of the larger source region of northwestern Africa (e.g. elevated contents of calcite and dolomite, occurrence of palygorskite).

3. Particles solely dominated by iron (Fe oxides and hydroxides) which are crucial for the optical properties of mineral dust and for the supply of nutrients to terrestrial and marine ecosystems are rare in our samples. However, small Fe-dominated grains (<500 nm) are often an important minor constituent of alumosilicate particles (clay mineral aggregates) and may change the absorption properties of these internally mixed aggregates.

4. Most particle groups exhibit median aspect ratios between 1.5 and 1.6. Higher aspect ratios are determined for internally mixed particles and for Cl- and S-dominated particles (except NaCl). Thus it can be concluded that higher fractions of internal mixtures in a dust aerosol will cause higher aspect ratios which in turn will change the radiative characteristics of the dust. Taken together with other studies, a trend of increasing aspect ratios with greater transport distances is observed for Northern African dust transported towards the Atlantic Ocean.

6. Acknowledgments

We want to thank the Royal Government of Morocco and the governors of the provinces of Zagora and Ouarzazate for their support, and Enviscope (Frankfurt a. M.) for logistic support and operation of the Partenavia aircraft. Financial support by the German Research Foundation (DFG project FOR 539) in the framework of the DFG research group SAMUM is gratefully acknowledged.

References

Alastuey, A., Querol, X., Castillo, S., Escudero, M., Avila, A. and co-authors. 2005. Characterisation of TSP and PM2.5 at Izaña and Sta. Cruz de Tenerife (Canary Islands, Spain) during a Saharan dust episode (July 2002). *Atmos. Environ.* **39**, 4715–4728.

Alfaro, S. C., Lafon, S., Rajot, J. L., Formenti, P., Gaudichet, A. and co-authors. 2004. Iron oxides and light absorption by pure desert dust: an experimental study. *J. Geophys. Res.* **109**, D08208, doi:10.1029/2003JD004374.

Arimoto, R. 2001. Eolian dust and climate: relationships to sources, tropospheric chemistry, transport and deposition. *Earth Sci. Rev.* **54**, 29–42.

Avila, A., Queralt-Mitjans, I. and Alarcón, M. 1997. Mineralogical composition of African dust delivered by red rains over northeastern Spain. *J. Geophys. Res.* **102**, D18, 21977–21996.

Berthier, S., Chazette, P., Couvert, P., Pelon, J., Dulac, F. and co-authors. 2006. Desert dust aerosol columnar properties over ocean and continental Africa from Lidar in-Space Technology Experiment (LITE) and Meteosat synergy. *J. Geophys. Res.* **111**, D21202, doi:10.1029/2005JD006999.

Blanco, A., De Tomasi, F., Filippo, E., Manno, D., Perrone, M. R. and co-authors. 2003. Characterization of African dust over southern Italy. *Atmos. Chem. Phys.* **3**, 2147–2159.

Bout-Roumazeilles, V., Combourieu Nebout, N., Peyron, O., Cortijo, E., Landais A. and co-authors. 2007. Connection between South Mediterranean climate and North African atmospheric circulation during the last 50,000 yr BP North Atlantic cold events. *Quarter. Sci. Rev.* **26**, 3197–3215.

Brust, J. and Waniek, J. J. 2010. Atmospheric dust contribution to deep-sea particle fluxes in the subtropical Northeast Atlantic. *Deep-Sea Res. I* **57**, 988–998.

Caquineau, S., Gaudichet, A., Gomes, L. and Legrand, M. 2002. Mineralogy of Saharan dust transported over northwestern tropical Atlantic Ocean in relation to source regions. *J. Geophys. Res.* **107** (D15), 4251, doi:10.1029/2000JD000247.

Chou, C., Formenti, P., Maille, M., Ausset, P., Helas, G. and co-authors. 2008. Size distribution, shape, and composition of mineral

dust aerosols collected during the African Monsoon Multidisciplinary Analysis Special Observation Period 0: dust and Biomass-Burning Experiment field campaign in Niger, January 2006. *J. Geophys. Res.* **113**, D00C10, doi:10.1029/2008JD009897.

Claquin, T., Schulz, M. and Balkanski, Y. J. 1999. Modeling the mineralogy of atmospheric dust sources. *J. Geophys. Res.* **104**, 22243–22256.

Coudé-Gaussen, G. 1989. Local, proximal and distal Saharan dusts: characterization and contribution to the sedimentation. In: *Paleoclimatology and Paleometeorology: Modern and Past Patterns of Global Atmospheric Transport* (eds M. Leinen and M. Sarnthein). NATO ASI Series, Kluwer Academic, Norwell, Mass., 339–358.

Coudé-Gaussen, G., Rognon, P., Bergametti, G., Gomes, L., Strauss, B. and co-authors. 1987. Saharan dust on Fuerteventura Island (Canaries): chemical and mineralogical characteristics, air mass trajectories, and probable sources. *J. Geophys. Res.* **92**, 9753–9771.

D'Almeida, G. A. 1986. A model for Saharan dust transport. *J. Clim. Appl. Meteorol.* **25**, 903–916.

Dentener, F. J., Carmichael, G. R., Zhang, Y., Lelieveld, J. and Crutzen, P. J. 1996. Role of mineral aerosol as a reactive surface in the global troposphere. *J. Geophys. Res.* **101**, D17, 22869–22889.

Desboeufs, K. V. and Cautenet, G. 2005. Transport and mixing zone of desert dust and sulphate over Tropical Africa and the Atlantic Ocean region. *Atmos. Chem. Phys. Discuss.* **5**, 5615–5644.

Dubovik, O., Sinyuk, A., Lapyonok, T., Holben, B. N., Mishchenko, M. and co-authors. 2006. The application of spheroid models to account for aerosol particle non-sphericity in remote sensing of desert dust. *J. Geophys. Res.* **111**, D11208, doi:10.1029/2005JD006619.

Engelstaedter, S., Tegen, I. and Washington, R. 2006. North African dust emissions and transport. *Earth-Sci. Rev.* **79**, 73–100.

FAO/IIASA/ISRIC/ISSCAS/JRC 2009. *Harmonized World Soil Database (version 1.1)*. FAO, Rome, Italy and IIASA, Laxenburg, Austria.

Formenti, P., Elbert, W., Maenhaut, W., Haywood, J. and Andreae, M. O. 2003. Chemical composition of mineral dust aerosol during the Saharan Dust Experiment (SHADE) airborne campaign in the Cape Verde region, September 2000. *J. Geophys. Res.* **108**, D18, 8576, doi:10.1029/2002JD002648.

Goudie, A. S. and Middleton, N. J. 2006. *Desert Dust in the Global System.* Springer Verlag, Berlin, 1–287.

Guieu, C., Bozec, Y., Blain, S., Ridame, C., Sarthou, G. and co-authors. 2002. Impact of high Saharan dust inputs on dissolved iron concentrations in the Mediterranean Sea. *Geophys. Res. Lett.* **29**, 1911, doi:10.1029/2001GL014454.

Heese, B., Althausen, D., Dinter, T., Esselborn, M., Müller, T. and co-authors. 2009. Vertically resolved dust optical properties during SAMUM: Tinfou compared to Ouarzazate. *Tellus* **61B**, 195–205.

Heintzenberg, J. 2009. The SAMUM-1 experiment over Southern Morocco: overview and introduction. *Tellus* **61B**, 2–11.

IPCC 2007. *Climate Change 2007: the Physical Science Basis – Contribution of Working Group I to the Fourth Assessment Report of the Intergovernmental Panel on Climate Change* (eds Solomon, S. et al.). Cambridge University Press, Cambridge, UK.

Jickells, T. D., An, Z. S., Andersen, K. K., Baker, A. R., Bergametti, G. and co-authors. 2005. Global iron connections between desert dust, ocean biogeochemistry, and climate. *Science* **308**, 67–71.

Kandler, K., Benker, N., Bundke, U., Cuevas, E., Ebert, M. and co-authors. 2007. Chemical composition and complex refractive index of Saharan Mineral Dust at Izaña, Tenerife (Spain) derived by electron microscopy. *Atmos. Environ.* **41**, 37, 8058–8074.

Kandler, K., Schütz, L., Deutscher, C., Ebert, M., Hormann, H. and co-authors. 2009. Size distribution, mass concentration, chemical and mineralogical composition and derived optical parameters of the boundary layer aerosol at Tinfou, Morocco, during SAMUM 2006. *Tellus* **61B**, 32–50.

Kandler, K., Lieke, K., Benker, N., Emmel, C., Küpper, M. and co-authors. 2011. Electron microscopy of particles collected at Praia, Cape Verde, during the Saharan mineral dust experiment: particle chemistry, shape, mixing state and complex refractive index. *Tellus* **63B**, this issue.

Knippertz P., Deutscher, C. Kandler, K. Müller, T. Schulz, O. and co-authors. 2007. Dust mobilization due to density currents in the Atlas region: observations from the Saharan Mineral Dust Experiment 2006 field campaign. *J. Geophys. Res.* **112**, D21109, doi:10.1029/2007JD008774.

Knippertz, P., Ansmann, A., Althausen, D., Müller, D., Tesche, M. and co-authors 2009. Dust mobilization and transport in the Northern Sahara during SAMUM 2006—a meteorological overview. *Tellus* **61B**, 12–31.

Krueger, B. J., Grassian, V. H., Cowin, J. P. and Laskin, A. 2004. Heterogeneous chemistry of individual mineral dust particles from different dust source regions: the importance of particle mineralogy. *Atmos. Environ.* **38**, 6253–6261.

Lafon, S., Sokolik, I. N., Rajot, J. L., Caquineau, S. and Gaudichet, A. 2006. Characterization of iron oxides in mineral dust aerosols: implications for light absorption. *J. Geophys. Res.* **111**, D21207, doi:10.1029/2005JD007016.

Laurent, B., Marticorena, B., Bergametti, G., Léon, J. F. and Mahowald, N. M. 2008. Modeling mineral dust emissions from the Sahara desert using new surface properties and soil database. *J. Geophys. Res.* **113**, D14218, doi:10.1029/2007JD009484.

Lieke, K., Kandler, K., Scheuvens, D., Emmel, C., von Glahn, C. and co-authors. 2011. Particle chemical properties in the vertical column based on aircraft observations in the vicinity of Cape Verde islands. *Tellus* **63B**, this issue.

Matsuki, A., Schwarzenboeck, A., Venzac, H., Laj, P., Crumeyrolle, S. and co-authors. 2010. Cloud processing of mineral dust: direct comparison of cloud residual and clear sky particles during AMMA aircraft campaign in summer 2006. *Atmos. Chemis. Phys.* **10**, 1057–1069.

Matthias-Maser, S. 1999. MOCIS, an automatic mobile cascade impaction system developed for use at ground and on airborne platforms and suitable for single particle analysis. *J. Aerosol Sci.* **30**(Suppl. 1), S367–S368.

Molinaroli, E. 1996. Mineralogical characterisation of Saharan dust with a view to its final destination in Mediterranean sediments. In: *The Impact of Desert Dust Across the Mediterranean* (eds Guerzoni, S. and Chester, R.). Kluwer Acad., Norwell, MA, 153–162.

Moreno, T., Querol, X., Castillo, S., Alastuey, A., Cuevas, E. and co-authors. 2006. Geochemical variations in aeolian mineral particles from the Sahara–Sahel Dust Corridor. *Chemosphere* **65**, 261–270.

Müller, D., Heinold, B., Tesche, M., Tegen, I., Althausen, D. and co-authors. 2009. EARLINET observations of the 14–22-May long-range dust transport event during SAMUM 2006: validation of results from dust transport modelling. *Tellus* **61B**, 325–339.

Nicolás, J., Chiari, M., Crespo, J., Garcia Orellana, I., Lucarelli, F. and co-authors. 2008. Quantification of Saharan and local dust impact in an arid Mediterranean area by the positive matrix factorization (PMF) technique. *Atmos. Environ.* **42**, 8872–8882.

Otto, S., Bierwirth, E., Weinzierl, B., Kandler, K., Esselborn, M. and co-authors. 2009. Solar radiative effects of a Saharan dust plume observed during SAMUM assuming spheroidal model particles. *Tellus* **61B**, 270–296.

Ozer, P., Ould Mohamed Laghdaf, M. B., Ould Mohamed Lemine, S. and Gassani, J. 2006. Estimation of air quality degradation due to Saharan dust at Nouakchott, Mauritania, from horizontal visibility data. *Water, Air, and Soil Pollution* **178**, 1–4, 79–87.

Paquet, H., Coudé-Gaussen, G. and Rognon, P. 1984. Etude minéralogique de poussières sahariennes le long d'un itinéraire entre 19° et 35° de latitude nord. *Rév. Géol. Dynamique et Géogr. Phys.* **25**, 257–265.

Petzold, A., Rasp, K., Weinzierl, B., Esselborn, M., Hamburger, T. and co-authors. 2009. Saharan dust absorption and refractive index from aircraft-based observations during SAMUM 2006. *Tellus* **61B**, 118–130.

Prospero, J. M., Barrett, K., Church, T., Dentener, F., Duce, R. A. and co-authors. 1996. Atmospheric deposition of nutrients to the North Atlantic Basin. *Biogeochemistry* **35**, 27–73.

Prospero, J. M., Ginoux, P., Torres, O., Nicholson, S. E. and Gill, T. E. 2002. Environmental characterization of global sources of atmospheric soil dust identified with the Nimbus 7 Total Ozone Mapping Spectrometer (TOMS) absorbing aerosol product. *Rev. Geophys.* **40**, 1002: doi:10.1029/2000RG00095.

Reid, E. A., Reid, J. S., Meier, M. M., Dunlap, M. R., Cliff, S. S. and co-authors. 2003. Characterization of African dust transported to Puerto Rico by individual particle and size segregated bulk analysis. *J. Geophys. Res.* **108**, 8591: doi:10.1029/2002JD002935.

Rognon, P., Coudé-Gaussen, G., Bergametti, G. and Gomes, L. 1989. Relationships between the characteristics of soils, the wind energy and dust near the ground, in the western sandsea (N.W. Sahara). In: *Paleoclimatology and Paleometeorology: Modern and Past Patterns of Global Atmospheric Transport* (eds Leinen, M. and Sarnthein, M.). Kluwer Acad., Norwell, Mass., 167–184.

Schepanski, K., Tegen, I., Todd, M. C., Heinold, B., Bönisch, G. and co-authors. 2009. Meteorological processes forcing Saharan dust emission inferred from MSG-SEVIRI observations of subdaily dust source activation and numerical models. *J. Geophys. Res.* **114**, D10201, doi:10.1029/2008JD010325.

Schütz, L. and Sebert, M. 1987. Mineral aerosols and source identification. *J. Aerosol Science* **18**, 1–10.

Sokolik, I. N. and Toon, O. B. 1999. Incorporation of mineralogical composition into models of the radiative properties of mineral aerosol from UV to IR wavelengths. *J. Geophys. Res.* **104**, D8, 9423–9444.

Sokolik, I. N., Winker, D. M., Bergametti, G., Gillette, D. A., Carmichael, G. and co-authors. 2001. Introduction to special section: outstanding problems in quantifying the radiative impacts of mineral dust. *J. Geophys. Res.* **106**, 18015–18027.

Stuut, J.-B., Zabel, M., Ratmeyer, V., Helmke, P., Schefuß, E. and co-authors. 2005. Provenance of present-day eolian dust collected off NW Africa. *J. Geophys. Res.* **110**, D04202, doi: 10.1029/2004JD005161.

Swap, R., Garstang, M., Greco, S., Talbot, R. and Kallberg, P. 1992. Saharan dust in the Amazon Basin. *Tellus* **44B**, 133–149.

Tesche, M., Ansmann, A., Müller, D., Althausen, D., Mattis, I. and co-authors. 2009. Vertical profiling of Saharan dust with Raman lidars and airborne HSRL in southern Morocco during SAMUM. *Tellus* **61B**, 144–164.

Verrecchia, E. P. and Le Coustumer, M.-N. 1996. Occurrence and genesis of palygorskite and associated clay minerals in a Pleistocene calcrete complex, Sde Boqer, Negev Desert, Israel. *Clay Miner.* **31**, 183–202.

Weigel, R. 2002. *Kalibrierung und Erprobung eines Impaktorsystems zur Bestimmung der vertikalen Größenverteilung von Aerosolpartikeln unter besonderer Berücksichtigung biologischer Teilchen*. MS Thesis, University of Mainz, Germany.

Weinzierl, B., Petzold, A., Esselborn, M., Wirth, M., Rasp, K. and co-authors. 2009. Airborne measurements of dust layer properties, particle size distribution and mixing state of Saharan dust during SAMUM 2006. *Tellus* **61B**, 96–117.

Wu, L. 2007. Impact of Saharan air layer on hurricane intensity. *Geophys. Res. Letters* **34**, L09802, doi:10.1029/2007GL029564.

Zhuang, H., Chan, C. K., Fang, M. and Wexler, A. S. 1999. Formation of nitrate and non-sea salt sulphate on coarse particles. *Atmos. Environ.* **33**, 4223–4233.

Zorn, S. 2005. *Optimierung des "Mobile Cascade Impaction System" für den Einsatz in ariden Gebieten*. MS Thesis, University of Mainz, Germany.